ISSN: 2634 - 8845

Journal of Earth and Environmental Sciences Research

SCIENTIFIC Research and Community

Review Article

Open Access

Seismic Hazard Indicators in Japan based on Seismic Noise Properties

Alexey Lyubushin

Institute of Physics of the Earth, Russia, Moscow

ABSTRACT

The seismic noise recorded at the network of stations in Japan for more than 26 years (1997 - March 2023) is being investigated. The article is a continuation of the number of works in which the analysis was performed for 1997 - March 2021. New data for 2 years of follow-up observations, combined with a new approach to their analysis, provided additional opportunities to test a number of hypotheses regarding the presence of features in the properties of seismic noise that precede the release of seismic energy. The analysis is based on the use of the wavelet-based Donoho-Johnstone index, as a property of noise waveforms, the use of an auxiliary network of reference points, the estimation of spatial correlations of noise properties, and the relationship of the seismic noise response to the irregular rotation of the Earth with the flow of seismic events in the vicinity of the Japanese Islands by using a parametric model of interacting point processes.

***Corresponding author**

Alexey Lyubushin, Institute of Physics of the Earth, Russia, Moscow.

Received: August 20, 2023; **Accepted:** August 27, 2023; **Published:** August 31, 2023

Keywords: Seismic Noise, Wavelet Analysis, Entropy, Donoho-Johnston Index, Correlations, Interaction of Point Processes, Irregularity of the Earth's Rotation.

Introduction

The article uses a property of seismic noise waveforms, which is known in wavelet analysis as the Donoho-Johnston index (DJ index). This concept is based on the value of the threshold separating large wavelet coefficients from other coefficients [1]. The DJ index itself is a dimensionless value equal to the ratio of the number of large wavelet coefficients to their total number. The experience of the author of the study of various properties of low-frequency seismic noise to search for changes in their properties of effects that precede strong earthquakes [2-8] showed that the DJ index has a number of advantages compared to other noise characteristics. This study presents new results of using the DJ index to analyze seismic noise in the Japanese Islands, supplementing the results obtained in, by increasing the length of the analyzed time interval by 2 years and using new noise characteristics (minimum histograms and a parametric model of interacting point processes) [6].

An essential element of the current seismic hazard is the use of the response of the seismic noise property to the irregularity of the Earth's rotation by the analysis of the correlation function between the released seismic energy and the coherence between the DJ index of seismic noise and the length of day time series.

Estimating the timing of the possible future mega-quake in Japan is based on the occurrence of seismic noise response to the Earth's rotation and the delay between the values of the response of noise to LOD and the seismic energy release in the region of the Japan Islands. The location of a possible next mega-earthquake is estimated from histograms of places of concentration of minimum values of seismic noise DJ-index.

The basis for a detailed study of the properties of seismic noise is the consideration that it is an important source of information about processes preceding strong earthquakes. The energy source of the Earth's seismic background is mainly the impact of atmospheric cyclones on the Earth's surface and ocean waves on the shelf and coast [9-15]. It is natural to assume that, since the earth's crust is a medium for the propagation of seismic waves, internal processes are reflected in changes in the statistical properties of seismic noise, and the study of these properties makes it possible to determine both the features of the structure of the earth's crust and changes in noise properties that precede strong earthquakes [2-8,16-18].

Initial Seismic Noise Data

We used 1 Hz vertical seismic data available from source http://www.fnet.bosai.go.jp/faq/?LANG=en (accessed on 04 April 2023) for 78 F-net seismic stations in Japan. The time interval from the beginning of 1997 to March 31, 2023 was considered. Figure 1 shows the location of the network stations. An auxiliary network of 16 reference points is introduced, the positions of which are determined using a cluster analysis of the positions of seismic stations using the "far neighbors" algorithm [19]. The seismic stations and reference points positions are shown in Figure 1. Reference points are numbered in decreasing order of their latitudes.

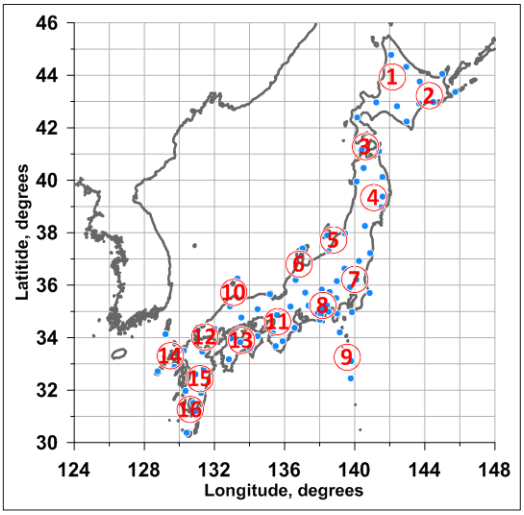

Figure 1: Positions of 78 seismic stations (blue circles) and a network of 16 reference points (numbered red circles).

Seismic Noise Waveforms Properties

Let's consider a random time series $x(t)$, $t = 1,.., N$ where t is an integer time index. The wavelet-based informational entropy of a finite sample is given by the formula:

$$En = -\sum_{k=1}^{N} p_k \cdot \log(p_k)/\log(N), \quad p_k = c_k^2 / \sum_{j=1}^{N} c_j^2 \qquad (1)$$

Here c_k are coefficients of orthogonal wavelet decomposition. The optimum wavelet basis is chosen from the minimum of entropy (1) among Daubechies wavelet bases [Mallat, 1999] with the number of vanishing moments from 1 to 10. The threshold T_{DJ} is defined by the formula [1]:

$$T_{DJ} = \sigma\sqrt{2 \cdot \ln N} \qquad (2)$$

The threshold (2) separates rather large (informative) in their absolute values wavelet coefficients from other coefficients which are considered to be noisy. Thus, we can consider the dimensionless signal characteristics γ, $0 < \gamma < 1$, as the ratio of the number of the most informative wavelet coefficients, for which the inequality $|c_k| > T_{DJ}$ is satisfied, to the total number N of all wavelet coefficients.

The value σ in the formula (2) is the noise standard deviation estimate under the assumption that the noise is most concentrated in the 1st detail level of orthogonal wavelet decomposition. The estimate of standard deviation σ should be robust with respect to outliers in the values of the coefficients at the first level. To provide this, a median estimate of the standard deviation for a normal random variable is used:

$$\sigma = med\left\{\left|c_k^{(1)}\right|, k = 1,..., N/2\right\} / 0.6745, \qquad (3)$$

where $c_k^{(1)}$ are wavelet coefficients at the first level of detail; $N/2$ is the number of such coefficients. The estimate of the standard deviation s from formula (3) determines the value (2) as a "natural" threshold for extracting noise wavelet coefficients. The quantity (2) is known in wavelet analysis as the Donoho–Johnstone threshold, and the expression for this quantity is based on the formula for the asymptotic probability of the maximum deviations of Gaussian white noise [1,20]. The DJ index γ values can be interpreted as a measure of the non-stationarity of seismic noise. For stationary Gaussian white noise, the index γ is zero.

For each reference point, the value of DJ index value is computed daily as a median from the 5 nearest working stations. Thus, time series with a uniform sampling step of 1 day at 16 reference points are obtained. Figure 2 shows the graphs of the DJ index for 4 reference points

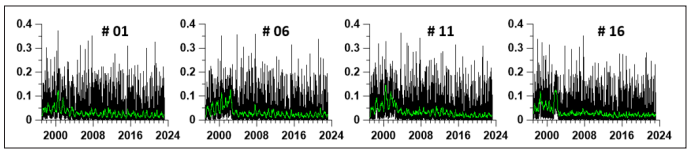

Figure 2: Daily values of DJ-index γ in 4 reference points, green lines - running average within time window of the length 57 days

Decreasing of the index γ means simplification of the statistical structure of noise (it becomes closer to white noise) what is associated with an increase in seismic hazard [3,4,6]. That is why the regions and time intervals with minimum values of γ are interested for estimating of seismic hazard. A simple way to estimate the variability of the probability density of extreme properties random signal is to construct histograms of the distribution of reference points numbers in which the statistics extrema are realized [8]. The construction of such histograms in a sliding time window makes it possible to determine the reference points at which the minimum values of the seismic noise DJ index are most often realized. This method provides possibility compactly visualize the temporal dynamics, for instance, to find the time intervals and sites when concentration of extreme values of the noise statistics change sharply. The number of histogram bins is taken equal to 16 what is the number of reference points. Such choice makes it possible to visualize the dynamics of the emergence and disappearance of bursts of the probability of extreme values at each reference point.

Figure 3: Histogram of numbers of reference points, in which the minimum values of the index γ were realized in a moving time window 365 days long.

The histogram in Figure 3 shows strips of probability concentration for the minimum values of the DJ index for data from the vicinity of control points with numbers 7-9 and 3-4. The highest concentration of minimum γ values is observed for the reference point #9 starting from 2004 until the end of the considered time interval. This behavior of the minimum values of the DJ index is interpreted as the existence of a permanent source of seismic hazard with an increased probability of strong earthquakes in the vicinity of reference point #9. Another high risk area corresponds to point #4, which emerged in 2002-2003 (taking into account that the estimates in Figure 3 are given for a 1-year time window) and ended in 2020. Note that the vicinity of reference point #4

is the area where the epicenter of the March 11, 2011 Tohoku mega-earthquake is located. The continuation of the line of increased probability of low γ values after 2011 for point #4 is associated with aftershock activity. Estimates of places of increased seismic hazard in Figure 3 coincide with the estimates previously given in [1], which were obtained by constructing maps of 2D probability densities of the distribution of extreme values of seismic noise properties using Gaussian kernel functions. As noted above, the histogram method, in addition to its simplicity, provides a more accurate determination of the times of occurrence and disappearance of seismic hazard [8].

Seismic Noise Response to Irregularity of Earth's Rotation

There is a connection between irregularity of Earth's rotation and seismic activity [21]. The triggering of irregular Earth's rotation to seismic process was studied in [22]. Direct effect of influence of strong earthquake on the length of the day was studied in [23]. Figure 4 shows a graph of the time series of the length of the day for the time interval 1997-2022.

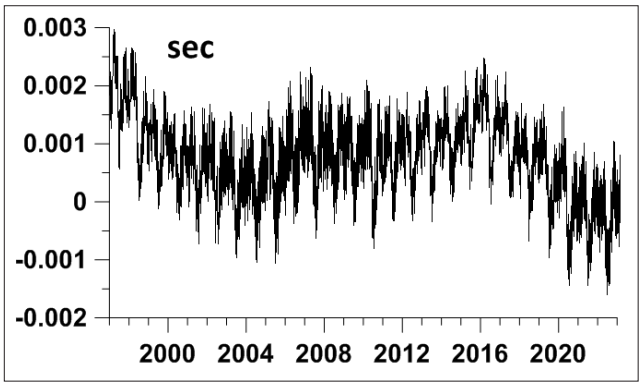

Figure 4: Time series plot of the length of a day for the time interval 1997-2023. LOD day length data is available from the website of International Earth rotation and Reference systems Service (IERS). Available online: https://hpiers.obspm.fr/iers/eop/eopc04/eopc04.1962-now (accessed on 04 April 2023)

We use the time series of length of days (LOD) as "input" for seismic noise properties for investigation of their responses in connection to seismicity [6,8,24,25]. The response is calculated as the maximum quadratic coherences between the LOD and seismic noise properties at each reference point. In this paper the coherences were estimated for 2 variants: (1) in moving time windows of 365 days with a shift of 3 days using a two-dimensional 5th order autoregressive model and (2) in moving time windows of the length 91 days (quarter of one year length) with the same shift 3 using autoregression of 3-rd order. Figure 5 shows examples of LOD response graphs at 4 reference points for two variants of moving time window length [26].

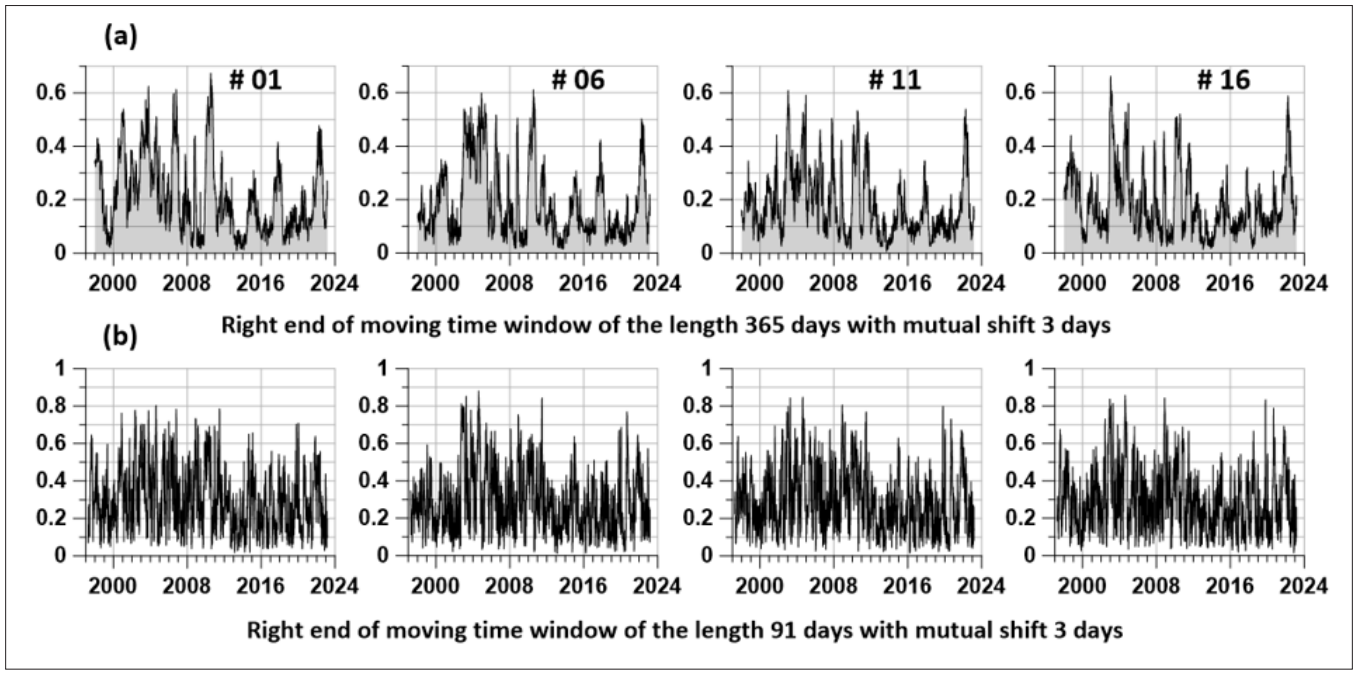

Figure 5: Plots of maximum coherence between index and LOD in a moving time window of 365 days (a) and 91 days (b) with mutual shift 3 days for 4 reference points.

Let us consider the integral response of seismic noise to a change in the length of the day by calculating the average values of coherences, the graphs of which are shown in Figures. 6(a) and compare this average response with the intensity of seismic energy release, which we represent as a sequence of logarithm values of energy in a sliding time window of 365 days with a shift of 3 days. The plots of Figure 6(a, b) show graphs of these dependencies. It is noticeable that the bursts of coherence in Figure 6(b) on average precede a significant release of seismic energy. The plot on Figure 6(c) is a graph of the correlation function between the curves in Figure 6(a, b) for time shifts of ±1200 days.

The graph of the correlation function in Figure 6(c) has a significant asymmetry and is shifted to the area of negative time shifts. This asymmetry corresponds to the average advance of the seismic noise response maxima per LOD of the maximum seismic energy bursts. The most probable advance can be defined as the value of the time shift at which the correlation function reaches its maximum. This shift is 426 days. This value of the correlation function shift has already been determined in for the observation interval 1997 - March 2021. The addition of 2 more years of observations, up to March 2023, made it possible to identify a new peak of the seismic noise response to LOD in 2022, which can precede a major earthquake with an average delay of 1.5 years [6].

The maximum value of the response in Figure 6(a) is reached at the time corresponding to the date 2022.04.06. The "direct" prediction, which uses addition of 426 days to this date, gives the most probable date for the future strong event on 2023.06.05. A realistic prediction should "smear" this date with some uncertainty interval. It is not yet possible to give such an interval due to the absence of the history of using the seismic noise response to LOD as a predictor.

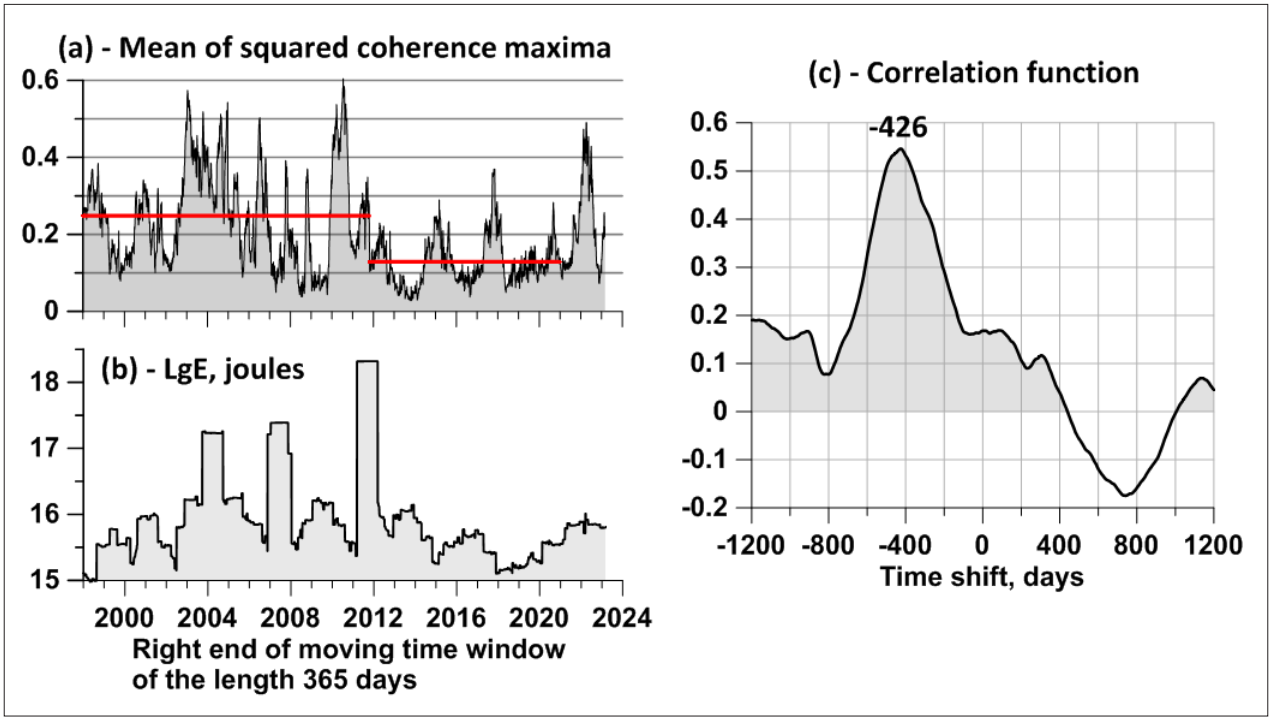

Figure 6(a) is the logarithm of the released seismic energy (in joules) within moving time window of the length 365 days with mutual shift 3 days; (b) – average values DJ-index response to LOD; (c) is the correlation function between the released seismic energy and DJ-index response to LOD.

Relationship Between Extrema Points of Noise Response to LOD and Strong Earthquakes

Another way to analyze the response of the seismic noise property (the average value of the DJ index) to the irregularity of the Earth's rotation (LOD – length of day time series), in addition to the already used estimate of the correlation function, consists in the mutual analysis of two event streams: earthquakes in the vicinity of the Japanese Islands with a magnitude of at least 6 and the points of the largest local maxima of the DJ-index response to LOD. It is for this purpose that the response was calculated over a shorter time window of 91 days, examples of which are shown in Figures 5(b), bottom row of graphs. The maximum response over all 16 reference points is presented in Figure 7(b), in which the red dots mark the 314 largest local maxima. The number 314 was chosen because it is the number of earthquakes with a magnitude of at least 6 for the considered time interval for the vicinity of the Japan Islands (Figure 1) is 314. The sequence of these seismic events is shown in Figure 7(a)

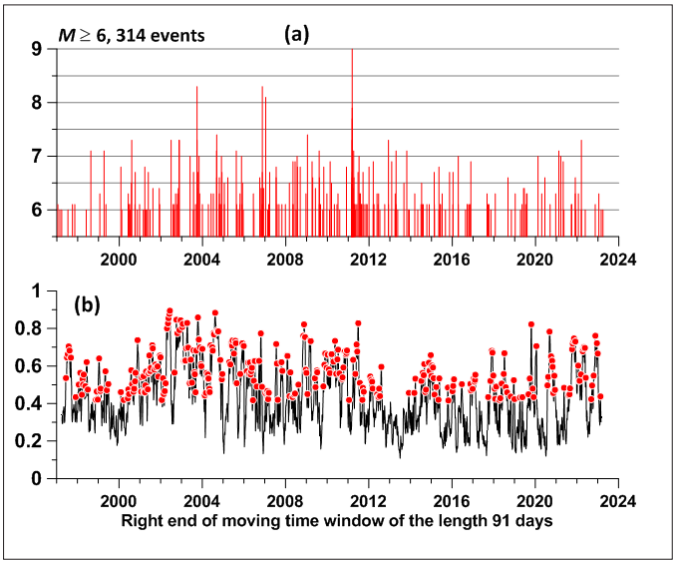

Figure 7(a) – sequence of 314 earthquakes with magnitudes in the vicinity of Japanese islands; (b) – maxima of maximum values of coherences between LOD and daily DJ-index values at 16 reference points within moving time window of the length 91 days with mutual shift 3 days, red points present the largest 314 local maxima values.

We want to study the relationship between two point processes, shown in Figure 7, in order to find features of relationships between event flows that can be interpreted as precursors of strong seismic events. A parametric model of the intensities of interacting point processes is used as an analysis tool. This model was used in for analyzing connections of strong earthquakes with extremal points of daily mean seismic noise properties including the DJ index [7].

Let $t_j^{(\alpha)}, j=1,...,N_\alpha; \alpha=1,2$ be of time moments of 2 sequences of events. The intensities of these series are presented in the form:

$$\lambda^{(\alpha)}(t)=b_0^{(\alpha)}+\sum_{\beta=1}^{2}b_\beta^{(\alpha)}\cdot g^{(\beta)}(t) \qquad (4)$$

where $b_0^{(\alpha)}\ge 0, b_\beta^{(\alpha)}\ge 0$ are parameters, $g^{(\beta)}(t)$ is a function of influence of the events $t_j^{(\beta)}$ from the stream with number β :

$$g^{(\beta)}(t)=\sum_{t_j^{(\beta)}<t}\exp(-(t-t_j^{(\beta)})/\tau) \qquad (5)$$

The formula (5) means that the weight of the event with the number j is non-zero for times $t_j^{(\beta)}$ and decays with the relaxation time τ. The parameter $b_\beta^{(\alpha)}$ determines the degree of influence of the flow β on the flow α. The parameter $b_\alpha^{(\alpha)}$ determines the self-exciting influence of the flow on itself, whereas corresponds to a purely random (Poisson) intensity share. The relaxation time is a free parameter. Let's consider the problem of determining the values $b_0^{(\alpha)}, b_\beta^{(\alpha)}$. The logarithmic likelihood functions for a non-stationary Poisson process at the time interval [0,T] is [27]:

$$\ln(L_\alpha)=\sum_{j=1}^{N_\alpha}\ln(\lambda^{(\alpha)}(t_j^{(\alpha)}))-\int_0^T\lambda^{(\alpha)}(s)ds,\quad \alpha=1,2 \qquad (6)$$

Let's consider the problem of seeking parameters $b_0^{(\alpha)}, b_\beta^{(\alpha)}$ from maximizing the function (6). The next expression could easily be obtained:

$$b_0^{(\alpha)}\frac{\partial\ln(L_\alpha)}{\partial b_0^{(\alpha)}}+\sum_{\beta=1}^{2}b_\beta^{(\alpha)}\frac{\partial\ln(L_\alpha)}{\partial b_\beta^{(\alpha)}}=N_\alpha-\int_0^T\lambda^{(\alpha)}(s)ds \qquad (7)$$

At the maximum point of function (6) each term on the left side of this formula is equal to zero. This follows from the conditions that parameters $b_0^{(\alpha)}, b_\beta^{(\alpha)}$ must be non-negative. Thus, if the parameters are positive at maximum point the partial derivatives equal zero from necessary extremum conditions or, if the maximum is reached at the boundary, then the parameters themselves are equal to zero. Therefore, at the maximum point of the likelihood function, the following equality holds:

$$\int_0^T\lambda^{(\alpha)}(s)ds=N_\alpha \qquad (8)$$

Substitute the expression $g^{(\beta)}(t)$ from (5) into (7) and divide by T. Then we get another form of formula (8):

$$b_0^{(\alpha)}+\sum_{\beta=1}^{m}b_\beta^{(\alpha)}\cdot\bar{g}^{(\beta)}=\lambda_0^{(\alpha)}\equiv N_\alpha/T \qquad (9)$$

where

$$\bar{g}^{(\beta)}=\int_0^T g^{(\beta)}(s)ds/T \qquad (10)$$

- the average value of the influence function. Substituting from (9) into (6), we obtain the following maximum problem:

$$\Phi^{(\alpha)}(b_1^{(\alpha)},b_2^{(\alpha)})=\sum_{j=1}^{N_\alpha}\ln(\lambda_0^{(\alpha)}+\sum_{\beta=1}^{2}b_\beta^{(\alpha)}\cdot\Delta g^{(\beta)}(t_j^{(\alpha)}))\to\max \qquad (11)$$

where $\Delta g^{(\beta)}(t)=g^{(\beta)}(t)-\bar{g}^{(\beta)}$, under the restrictions:

$$b_1^{(\alpha)}\ge 0, b_2^{(\alpha)}\ge 0, \sum_{\beta=1}^{2}b_\beta^{(\alpha)}\bar{g}^{(\beta)}\le\lambda_0^{(\alpha)} \qquad (12)$$

Function (12) is convex with a negative definite Hessian and, therefore, problem (11-12) has a unique solution and is solving numerically for a given relaxation time τ, Then the influence matrix elements $\kappa_\beta^{(\alpha)}, \alpha=1,2;\ \beta=0,1,2$ according to the formulas:

$$\kappa_0^{(\alpha)}=\frac{b_0^{(\alpha)}}{\lambda_0^{(\alpha)}}\ge 0,\quad \kappa_\beta^{(\alpha)}=\frac{b_\beta^{(\alpha)}\cdot\bar{g}^{(\beta)}}{\lambda_0^{(\alpha)}}\ge 0 \qquad (13)$$

The value $\kappa_0^{(\alpha)}$ is the pure random share of the mean intensity $\lambda_0^{(\alpha)}$ of the process , the share is the self-excitation part of intensity $\alpha\to\alpha$ and $\kappa_\beta^{(\alpha)}, \beta\ne\alpha$ is the share due to mutual exciting $\beta\to\alpha$. Formula (8) provides the normalization condition:

$$\kappa_0^{(\alpha)} + \sum_{\beta=1}^{2} \kappa_\beta^{(\alpha)} = 1, \quad \alpha = 1,2 \tag{14}$$

Finally, the influence matrix of the size 3x2 could be defined:

$$\left(\begin{vmatrix} \kappa_0^{(1)} \\ \kappa_0^{(2)} \end{vmatrix} \begin{vmatrix} \kappa_1^{(1)} & \kappa_2^{(1)} \\ \kappa_1^{(2)} & \kappa_2^{(2)} \end{vmatrix} \right) \tag{15}$$

First column of the matrix (15) is composed of Poisson shares of mean intensities. The diagonal elements of the right sub-matrix of the size 2x2 is composed of self-exciting shared of mean intensities whereas non-diagonal elements correspond to mutual-exciting. The sums of row components of influence matrix (15) are equal to 1.

Figure 8 shows the graphs of the behavior of the components of the influence matrix for assessing the relationship between sequences of earthquake events with a magnitude of at least 6 and the time points for reaching the largest local maxima of the DJ-index response to LOD, when assessed in a sliding time window of 4 years with a shift of time windows of 18 days (0.05 year) with the relaxation time parameter equal to 0.5 year. Of main interest is the component of the influence matrix, which describes influence of the sequence of local maxima of the DJ-index response to LOD on the sequence of earthquakes, since it is precisely this component that has an obvious application for forecasting purposes. The graph of this component is shown in Fig. 9(b1). This graph shows spikes in the influence component prior to the time of the Tohoku mega-quake. In addition, at the end of the processed time interval, a strong increase is also noticeable, which corresponds to the conclusion about the increased seismic hazard from the graphs in Fig.6.

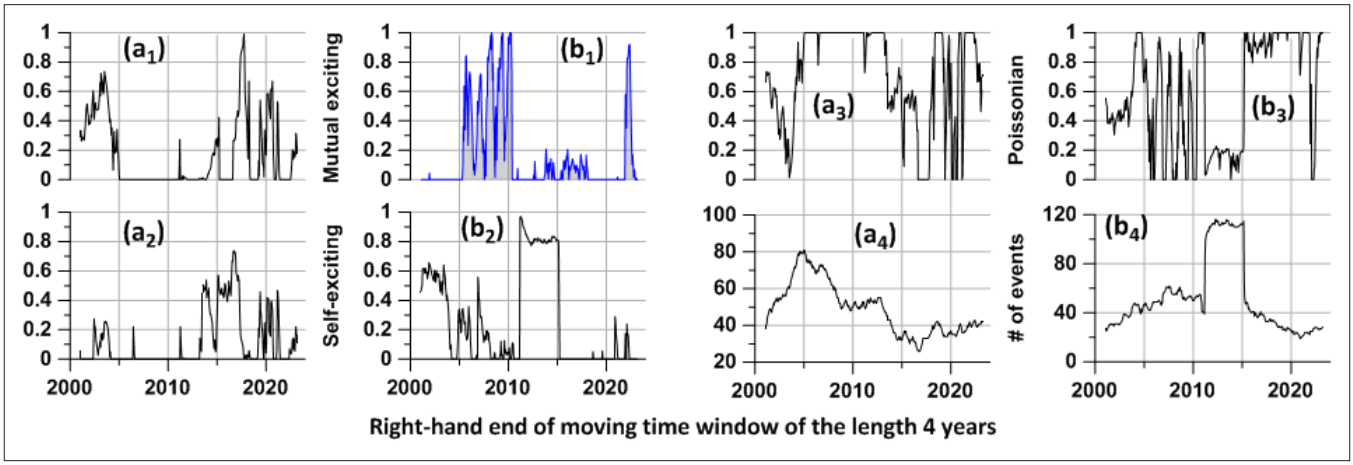

Figure 8: Components of influence matrix for estimation of relations between the sequence of maxima seismic noise DJ index average response per LOD and the sequence of earthquakes within vicinity of Japan islands. Left panel of graphs corresponds to the influence of coherence maxima sequence from sequence of seismic events whereas right panel of graphs corresponds to vice versa influence of seismic events from coherence maxima. Intensity shares were estimated within moving time window of the length 4 years, relaxation time of the intensity model was taken 0.5 years. Graphs (a1) and (b1) present mutual exciting components of influence matrix; (a2) and (b2) – self-exciting components, (a3) and (b3) – Poisson shares of intensities; (a4) and (b4) – numbers of events within each time window.

However, the graph in Figure 9(b1) refers only to the choice of a window length of 4 years. The question arises as to how stable the predictor effect, noticeable at 9(b1), is with respect to a change in the window length. To answer this question, we single out the moments of time corresponding to the local maxima of the influence matrix component when estimating a certain length in a sliding time window when it is shifted along the time axis. In Figure 9, the vertical segments represent the local maxima of the influence matrix component, corresponding to the graph in Figure 9(b1) for a window length of 4 years.

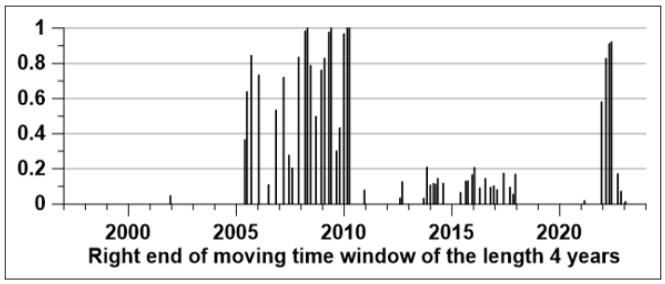

Figure 9: Vertical lines - positions on the time axis and values of local maxima of elements of the matrix of influence corresponding to the "influence" of the sequence of maxima seismic noise DJ index average response per LOD on sequence earthquakes for evaluation in a sliding time window of 4 years with a shift of 0.05 years, the relaxation time parameter is 0.5 years. The number of local maxima is 56.

Let's repeat this procedure for a set of lengths of time windows within some given limits. Below are taken 100 lengths of time windows ranging from 3 to 6 years. For each length, vertical segments on the time axis are determined, the length of which is equal to the value of the local maxima of the influence matrix component. The result is shown in Figure 10 for two options for choosing local maxima: (a) when using all local maxima in each time window and (b) when using the 10 largest local maxima.

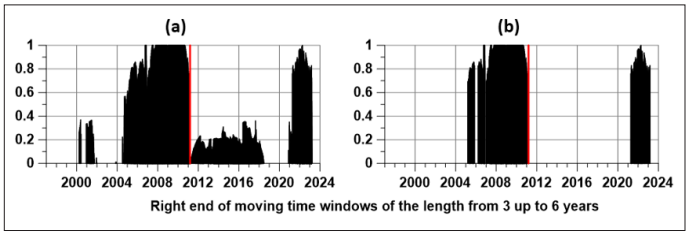

Figure 10: The times and magnitudes of local maxima of the matrices of the influence of the seismic noise index DJ responses on the LOD on the sequence of earthquakes $M \geq 6$ when estimating in moving time windows of lengths varying from 3 to 6 years with a shift of 0.05 years, the relaxation time in the model is = 0.5 years. The vertical red line corresponds to the time of the March 11, 2011 mega-earthquake. Plot (a) corresponds to using all local maxima of influence matrix component whereas plot (b) corresponds to using of 10 maximum local maxima in each time window.

For both options for choosing local maxima of the influence matrix component, it can be seen that these maxima are concentrated before the March 11, 2011 mega-earthquake. Further, the time interval of a significant concentration of the maximum values of this component of the influence matrix falls on the time marks of the right ends of the time windows, starting from mid-2021.

The interpretation of this feature, by analogy with the previous behavior, allows us to conclude that the Japanese islands are currently in a state of increased seismic hazard. According to the distribution histogram of the minimum values of the DJ-index in Fig. 3, the vicinity of the reference point 9 is the area of greatest danger.

Note that the possibility of a strong earthquake in the south of Japan, in the area of the junction of the Philippine oceanic plate with the Eurasian plate, has long been discussed among Japanese seismologists [28, 29]. Based on the analysis of data after the Tohoku mega-earthquake on March 11, 2011, it was concluded in that the probability of a strong earthquake shifted to the south of the aftershock cloud of the Tohoku earthquake (and this is just the vicinity of point #9) [30]. In, based on a retrospective analysis of seismic catalogs, it was shown that the conclusion about a high probability of an earthquake with a magnitude of 9 off the coast of Japan was quite possible based on data before 2011 [31]. In, the estimate of the maximum possible magnitude for seismic events in the Japan Trench was increased up to 10 [32].

Conclusions

The experience of using various statistics of low-frequency seismic noise to search for features of noise behavior that can be preceded by strong earthquakes unexpectedly showed that a relatively simple quantity describing the ratio of the number of "large" wavelet coefficients to their total number surpasses such properties as entropy in its efficiency or the support width of the multi-fractal spectrum of the singularity. For this reason, in this article, we focused on studying only the properties of the DJ index, although earlier the first principal component of three properties was used for the seismic noise of Japan: the DJ index, the entropy of the distribution of the squares of the wavelet coefficients, and the singularity spectrum support width [6]. At the same time, the previously used method for estimating spatial distribution maps of extreme properties of seismic noise using a kernel Gaussian estimate was also replaced by a simpler method for calculating the histogram of the distribution of reference points numbers, in which the minimum of the DJ index was realized in a sliding time window. This method of representing the variability of the distribution over space of the minimum values of the DJ index, in addition to its ease of implementation, makes it possible to present the temporal dynamics of this variability in a compact form. Inclusion in the analysis of new data 2 years in length compared to previous estimates led to the discovery of a significant spike in the response of the DJ index to LOD in 2022. This gives grounds to put forward a hypothesis about an increase in the current seismic hazard in the Japanese Islands, and the evaluation of the correlation function between the response to LOD and the release of seismic energy gives an approximate estimate of the time of a possible strong seismic shock. The use of a parametric model of two interacting point processes - a sequence of earthquakes with a magnitude of at least 6 and time points of the largest local maxima of the response to LOD, when assessed in a moving window of 91 days, also independently confirmed the hypothesis that the Japanese Islands would enter a dangerous time interval in 2022-2023. As for the place of a possible strong earthquake, according to the histogram of the change in the distribution over space of the minimum values of the DJ-index, the most probable place is the vicinity of reference point #9.

Funding: This research received no external funding

Data Availability Statement: The open access data from the sources: https://www.fnet.bosai.go.jp/faq/?LANG=en , https://hpiers.obspm.fr/iers/eop/eopc04/eopc04.1962-now https://earthquake.usgs.gov/earthquakes/search/ were used.

Acknowledgments: The work was carried out within the framework of the state assignment of the Institute of Physics of the Earth of the Russian Academy of Sciences (topic FMWU-2022-0018).

Conflicts of Interest: The author declares no conflict of interest.

References

1. DL, Johnstone IM (1995) Adapting to unknown smoothness via wavelet shrinkage, J. Am. Stat. Assoc 90: 1200-1224.
2. Lyubushin A (2012) Prognostic properties of low-frequency seismic noise. Natural Science 4: 659-666.
3. Lyubushin AA (2014) Dynamic estimate of seismic danger based on multifractal properties of low-frequency seismic noise. Natural Hazards 70: 471-483.
4. Lyubushin A (2018) Synchronization of Geophysical Fields Fluctuations. In Complexity of Seismic Time Series: Measurement and Applications, Editors: Tamaz Chelidze, Luciano Telesca, Filippos Vallianatos, Elsevier 2018, Amsterdam, Oxford, Cambridge. Chapter 6: 161-197.
5. Lyubushin A (2021a) Global Seismic Noise Wavelet-based Measure of Nonstationarity, Pure and Applied Geophysics 178: 3397-3413.
6. Lyubushin A (2021b) Low-Frequency Seismic Noise Properties in the Japanese Islands, Entropy 23: 4.
7. Lyubushin A (2022) Investigation of the Global Seismic Noise Properties in Connection to Strong Earthquakes . Front. Earth Sci. 10: 905663.
8. Lyubushin A (2023) Spatial Correlations of Global Seismic Noise Properties. Appl. Sci 13: 6958.
9. Ardhuin F, Stutzmann E, Schimmel M, Mangeney A (2011) Ocean wave sources of seismic noise, J. Geophys. Res 116: C09004.
10. Aster R, McNamara D, Bromirski P (2008) Multidecadal climate induced variability in microseisms, Seismol. Res. Lett 79: 194-202.
11. Friedrich A, Kruger F, Klinge K (1998) Ocean-generated microseismic noise located with the Grafenberg array, J. Seismol 2: 47-64.
12. Kobayashi N, Nishida K (1998) Continuous excitation of planetary free oscillations by atmospheric disturbances. Nature 395: 357-360.
13. Koper KD, Seats K, Benz H (2010) On the composition of Earth's short-period seismic noise field, Bull. Seismol. Soc. Am 100: 606-617.
14. Rhie J, Romanowicz B (2004) Excitation of Earth's continuous free oscillations by atmosphere-ocean-seafloor coupling, Nature 431: 552-554.
15. Tanimoto T (2005) The oceanic excitation hypothesis for the continuous oscillations of the Earth, Geophys. J. Int 160: 276-288.
16. Berger J, Davis P, Ekstrom G (2004) Ambient earth noise: a survey of the global seismographic network, J. Geophys. Res 109: B11307.
17. Fukao YK, Nishida K, Kobayashi N (2010) Seafloor topography, ocean infragravity waves, and background Love and Rayleigh waves. J. Geophys. Res 115: B04302.
18. Nishida K, Montagner J, Kawakatsu H (2009) Global surface wave tomography using seismic hum, Science 326 : 112.
19. Duda RO, Hart PE, Stork DG (2000) Pattern Classification, Wiley-Interscience Publication, New York, Chichester, Brisbane, Singapore, Toronto https://cds.cern.ch/record/683166/files/0471056693_TOC.pdf.
20. Mallat SA (1999) Wavelet Tour of Signal Processing. 2nd edition. Academic Press. San Diego, London, Boston, New York, Sydney, Tokyo, Toronto file:///C:/Users/SRC/Downloads/A_Wavelet_Tour_of_Signal_Processing.pdf.
21. Bendick R, R Bilham (2017) Do weak global stresses synchronize earthquakes? Geophys. Res. Lett 44: 8320-8327.
22. Shanker D, Kapur N, Singh V (2001) On the spatio temporal distribution of global seismicity and rotation of the Earth - A review, Acta Geod. Geoph. Hung 36: 175-187.
23. Xu Changy, Sun Wenke (2012) Co-seismic Earth's rotation change caused by the 2012 Sumatra earthquake, Geodesy and Geodynamics 3: 28-31.
24. Lyubushin A (2020a) Connection of Seismic Noise Properties in Japan and California with Irregularity of Earth's Rotation. Pure Appl. Geophys 177: 4677-4689.
25. Lyubushin A (2020b) Global Seismic Noise Entropy. Frontiers in Earth Science 8: 611663.
26. Marple SL (Jr) (1987) Digital spectral analysis with applications. 1987, Prentice-Hall, Inc., Englewood Cliffs, New Jersey https://www.amazon.com/Digital-Spectral-Analysis-Applications-Processing/dp/0132141493.
27. Cox DR, Lewis PAW (1966) The statistical analysis of series of events. London, Methuen 154: 757.
28. Mogi K (2004) Two grave issues concerning the expected Tokai Earthquake, Earth, Planets and Space 56: li-lxvi.
29. Rikitake T (1999) Probability of a great earthquake to recur in the Tokai district, Japan: reevaluation based on newly-developed paleoseismology, plate tectonics, tsunami study, micro-seismicity and geodetic measurements, Earth, Planets and Space 51: 147-157.
30. Simons M, Minson SE, Sladen A, Ortega F, Jiang J, et al. (2011) The 2011 Magnitude 9.0 Tohoku-Oki earthquake: mosaicking the megathrust from seconds to centuries, Science 332: 911.
31. Kagan YY, DD Jackson (2013) Tohoku Earthquake: A Surprise? Bulletin of the Seismological Society of America 103: 1181-1194.
32. Zoller G, Holschneider M, Hainzl S, Zhuang J (2014) The largest expected earthquake magnitudes in Japan: the statistical perspective, Bull. Seismol. Soc. Am 104: 769-779.